TU Delft

Delft University of Technology

Lengthening of the Sm^{2+} $4f^5 5d \rightarrow 4f^6$ decay time through interplay with the $4f^6[^5D_0]$ level and its analogy to Eu^{2+} and Pr^{3+}

van Aarle, Casper; Krämer, Karl W.; Dorenbos, Pieter

DOI
10.1016/j.jlumin.2023.120329

Publication date
2024

Document Version
Final published version

Published in
Journal of Luminescence

Citation (APA)
van Aarle, C., Krämer, K. W., & Dorenbos, P. (2024). Lengthening of the Sm^{2+} $4f^5 5d \rightarrow 4f^6$ decay time through interplay with the $4f^6[^5D_0]$ level and its analogy to Eu^{2+} and Pr^{3+}. *Journal of Luminescence*, *266*, Article 120329. https://doi.org/10.1016/j.jlumin.2023.120329

Important note
To cite this publication, please use the final published version (if applicable).
Please check the document version above.

Copyright
Other than for strictly personal use, it is not permitted to download, forward or distribute the text or part of it, without the consent of the author(s) and/or copyright holder(s), unless the work is under an open content license such as Creative Commons.

Takedown policy
Please contact us and provide details if you believe this document breaches copyrights.
We will remove access to the work immediately and investigate your claim.

This work is downloaded from Delft University of Technology.
For technical reasons the number of authors shown on this cover page is limited to a maximum of 10.

Journal of Luminescence 266 (2024) 120329

Contents lists available at ScienceDirect

Journal of Luminescence

journal homepage: www.elsevier.com/locate/jlumin

Full Length Article

Lengthening of the Sm^{2+} $4f^55d \rightarrow 4f^6$ decay time through interplay with the $4f^6[^5D_0]$ level and its analogy to Eu^{2+} and Pr^{3+}

Casper van Aarle [a,*], Karl W. Krämer [b], Pieter Dorenbos [a]

[a] Faculty of Applied Sciences, Delft University of Technology, Mekelweg 15, Delft, the Netherlands
[b] Department of Chemistry and Biochemistry, University of Bern, Freiestrasse 3, Bern, Switzerland

A B S T R A C T

Recent research activity on Sm^{2+}-doped compounds has significantly increased the amount of available data on $4f^55d \rightarrow 4f^6$ decay times. This enabled the systematic comparison of spectroscopic and time resolved luminescence data to theoretical models describing the interplay between the $4f^55d$ and $4f^6[^5D_0]$ excited states on the observed decay time. A Boltzmann distribution between the population of the excited states is assumed, introducing a dependence of the observed $4f^55d \rightarrow 4f^6$ decay time on the energy gap between the $4f^55d$ and $4f^6[^5D_0]$ levels and temperature. The model is used to interpret the origin of the large variation in reported $4f^55d \rightarrow 4f^6$ decay times through literature, and links their temperature dependence to applications such as luminescence thermometry and near-infrared scintillation. The model is further applied to the analogous situation of close lying $4f^{n-1}5d$ and $4f^n$ states in Eu^{2+} ($^6P_{7/2}$) and Pr^{3+} ($^1S_0$).

1. Introduction

Sm^{2+}-doped compounds have been explored for many purposes throughout the past decades. Spectroscopic data on Sm^{2+} has been valuable for fundamental understanding of the lanthanide energy levels in compounds and the electronic transitions between them [1–3]. Applications such as spectral hole burning for digital memory [4,5], solid state lasers [6–8], X-ray storage phosphors [9,10], luminescent solar concentrators [11,12], and pressure sensors [13–15] have been explored. In recent years, two of the most researched topics are the development of near-infrared scintillators [16–19] and luminescence thermometers [20–22].

A configurational coordinate diagram showing the energy levels of Sm^{2+} is shown in Fig. 1. The ground state is $4f^6[^7F_0]$, which is part of the $4f^6[^7F_J]$ multiplet. About 14,500 cm^{-1} above the ground state lies the $4f^6[^5D_0]$ level. Sm^{2+} can show emission from the $4f^6[^5D_0] \rightarrow 4f^6[^7F_J]$ transitions yielding multiple narrow emission lines ranging from 680 nm to 850 nm, each line corresponding to a different $4f^6[^7F_J]$ final state. The energy difference between the $4f^6$ levels is almost independent of host compound and therefore the emission lines always lie at approximately the same wavelength.

Sm^{2+} also has states of the $4f^55d$ configuration that lie close to the $4f^6[^5D_0]$ level. In this work, only the lowest $4f^55d$ level is considered, the energy of which does strongly depend on compound and can therefore be located at higher or lower energies than drawn in Fig. 1. In some compounds, Sm^{2+} shows $4f^55d \rightarrow 4f^6$ broad band emission instead of the $4f^6 \rightarrow 4f^6$ line emission. This happens when the $4f^55d$ states lies below the $4f^6[^5D_0]$ level or low enough that it is thermally populated, which is the case when the $4f^55d \rightarrow 4f^6$ emission lies at approximately 670 nm or longer wavelength [23]. Many of the compounds in which the $4f^55d \rightarrow 4f^6$ emission wavelength lies around this transition point at 670 nm still show $4f^6 \rightarrow 4f^6$ line emission at cryogenic temperatures.

Luminescence thermometry relies on measuring a property Q of the luminescent centre with known dependence on the temperature T. For Sm^{2+}-based thermometers, Q is often chosen to be the luminescence intensity ratio (LIR) between the $4f^55d \rightarrow 4f^6$ and $4f^6 \rightarrow 4f^6$ emission [24,25], or the decay time τ of any of the two emissions [26]. It is desired that Q varies strongly with temperature as this allows for more sensitive temperature measurement. This can be expressed as a figure of merit called the relative sensitivity.

$$S_r = \left| \frac{1}{Q} \frac{dQ}{dT} \right| \times 100\% \quad (1)$$

Both when using LIR or τ as measured property, compounds are typically selected where the $4f^55d$ level lies above the $4f^6[^5D_0]$ level. In that case, thermal excitation from the long lived $4f^6[^5D_0]$ level with a radiative lifetime time of milliseconds to the $4f^55d$ level with a radiative lifetime of microseconds causes large changes in τ upon temperature increase and simultaneously the spectrum rapidly changes from $4f^6 \rightarrow 4f^6$ line emission to broad band $4f^55d \rightarrow 4f^6$ emission [27,28].

* Corresponding author.
E-mail address: c.vanaarle@tudelft.nl (C. van Aarle).

https://doi.org/10.1016/j.jlumin.2023.120329
Received 14 September 2023; Received in revised form 16 November 2023; Accepted 19 November 2023
Available online 24 November 2023
0022-2313/© 2023 The Author(s). Published by Elsevier B.V. This is an open access article under the CC BY license (http://creativecommons.org/licenses/by/4.0/).

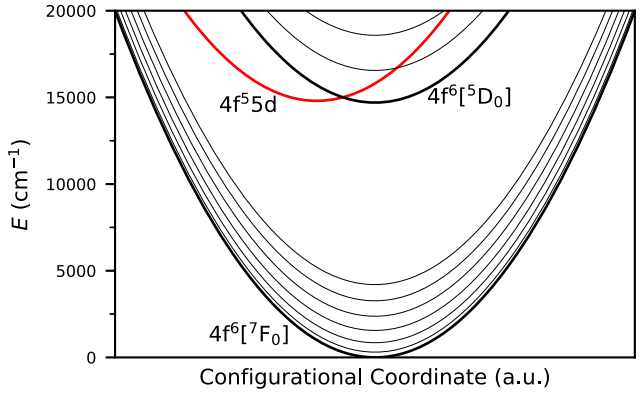

Fig. 1. Configurational coordinate diagram of Sm^{2+}. The black parabolas are $4f^6$ states, the red parabola is the $4f^5 5d$ state.

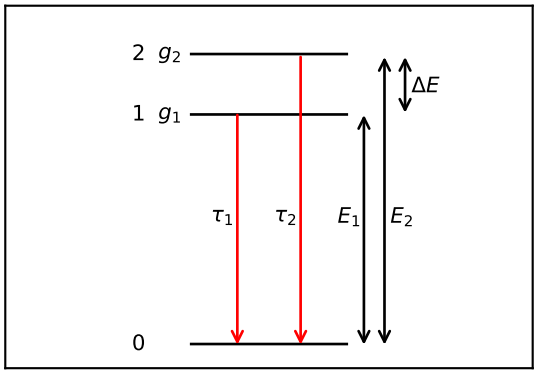

Fig. 2. 3 level system with ground state 0 and excited states 1 and 2. Excited states 1 (here, Sm^{2+} $4f^6[^5D_0]$) and 2 (Sm^{2+} $4f^5 5d$) are in thermal equilibrium and their respective degeneracies are g_1 and g_2. Their intrinsic lifetimes are τ_1 and τ_2. $\Delta E \equiv E_2 - E_1$ is the energy difference between the excited states.

For the development of near-infrared scintillators, Sm^{2+} is a promising activator as its emission wavelength is efficiently detected by silicon based photodetectors such as avalanche photodiodes and silicon photomultipliers [18]. It can be doped in the same hosts as the more conventional Eu^{2+} activator and can even be used as co-dopant to solve the self-absorption problems that Eu^{2+}-doped scintillators typically face [29]. For scintillator applications, it is necessary that the compound emits its light quickly, so that the scintillator is ready to detect a new γ-ray without overlap of the scintillation pulses. This means the $4f^5 5d \rightarrow 4f^6$ emission with its short τ is desirable and therefore development of near-infrared scintillators has largely focused on compounds in which the $4f^5 5d$ level lies below the $4f^6[^5D_0]$ level.

As the energy difference between the $4f^6$ levels is almost independent of compound, the energy difference between the $4f^5 5d$ level and the $4f^6[^5D_0]$ level can be conveniently approximated by only knowing the $4f^5 5d \rightarrow 4f^6$ emission wavelength. One problem is however that compounds which show exclusively $4f^5 5d \rightarrow 4f^6$ emission at room temperature still shows large variation in τ. Values have been reported between 1.5 μs [30] and 35 μs [31]. For scintillator applications such as γ-ray spectroscopy, an order of magnitude slower decay time is extremely undesirable, underlining the importance of a reliable prediction for τ. Unfortunately, the mechanism behind this large variation in τ has not yet been studied.

Feofilov and Tolstoi showed that a level system of two excited states in thermal equilibrium can be used to describe the temperature dependence of the Sm^{2+} decay time. The system is shown schematically in Fig. 2. State 1 lies at energy E_1 above the ground state, has degeneracy g_1 and an intrinsic radiative lifetime τ_1. The same applies to State 2, having its own energy E_2, degeneracy g_2 and intrinsic lifetime τ_2. The

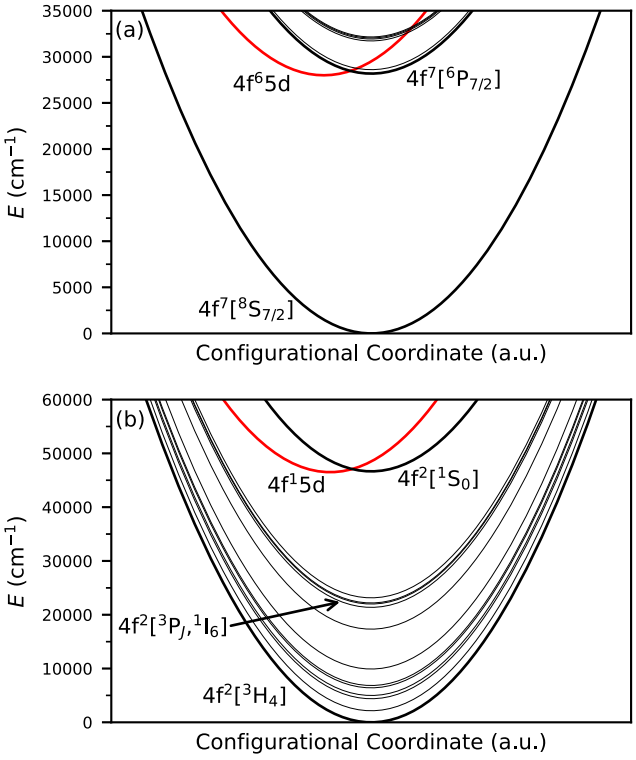

Fig. 3. Configurational coordinate diagram of a) Eu^{2+} and b) Pr^{3+}. The black parabolas are $4f^6$ states, the red parabolas are their respective $4f^{n-1}5d$ states.

energy difference between States 1 and 2 is defined as $\Delta E = E_2 - E_1$. When both excited states are in thermal equilibrium, emission from both states will have the same decay time, which is given by Equation (2) [32].

$$\tau(T, \Delta E) = \frac{1 + \frac{g_2}{g_1} e^{\frac{-\Delta E}{kT}}}{\tau_1^{-1} + \tau_2^{-1} \frac{g_2}{g_1} e^{\frac{-\Delta E}{kT}}} \tag{2}$$

When using this system to describe Sm^{2+}, State 1 and 2 correspond to the $4f^6[^5D_0]$ and $4f^5 5d$ states, respectively. The model assumes that all transitions to the ground state are radiative and thermal population of other levels such as the close lying $4f^6[^5D_1]$ state is neglected. Equation (2) has been successfully used to model the temperature dependence of the decay time of Sm^{2+} emission in many compounds of the MX_2 (M = Ca, Sr, Ba; X = F, Cl, Br) family, which often show a transition from $4f^6 \rightarrow 4f^6$ line emission to $4f^5 5d \rightarrow 4f^6$ broad band emission upon increase of temperature [32–35].

Showing $4f^{n-1}5d \rightarrow 4f^n$ broad band emission in some compounds and $4f^n \rightarrow 4f^n$ line emission in others is not exclusively a property of Sm^{2+}, as it is also observed for Eu^{2+} and Pr^{3+}. Fig. 3a shows a configurational coordinate diagram for Eu^{2+}. In most compounds, the $4f^6 5d$ level lies well below the $4f^7[^6P_{7/2}]$ level and only $4f^6 5d \rightarrow 4f^7$ emission is observed. When the $4f^6 5d$ level lies above 28,500 cm^{-1}, such as in SrFCl and BaFCl, $4f^7[^6P_{7/2}] \rightarrow 4f^7[^8S_{7/2}]$ line emission can be observed [36,37]. This mostly happens at 78 K or lower temperatures, as the distance between the $4f^6 5d$ and $4f^7[^6P_{7/2}]$ level is typically smaller than 500 cm^{-1}. Some examples of compounds in which emission from the $4f^7[^6P_{7/2}]$ level is observed at room temperature are reported in literature [38–44], most of which belong to the $AMgF_3$ (A = Na, K, Rb, Cs) family of compounds. It is believed that in these compounds the $4f^6 5d$ level is located more than 1000 cm^{-1} above the $4f^7[^6P_{7/2}]$ level because Eu^{2+} occupies the monovalent A cation site with small crystal field splitting. It has been reported that in some compounds where the $4f^6 5d$ level lies close to the $4f^7[^6P_{7/2}]$ level, the Eu^{2+} $4f^6 5d \rightarrow 4f^7$

emission decay time becomes longer than the typical intrinsic Eu^{2+} decay time of 0.5 μs to 1 μs [45,46]. For these compounds, Equation (2) has been used to determine ΔE between the $4f^6 5d$ and $4f^7[^6P_{7/2}]$ level from the $4f^6 5d \rightarrow 4f^7$ emission decay time [44,47,48]. This shows that the transition from broad band emitters to line emitters in Eu^{2+} is analogous to that of Sm^{2+}. Of the dopants discussed in this work, Eu^{2+} is the one for which by far the most spectroscopic data is available. The temperature dependence of its emission intensities and decay times have been extensively reviewed by Adachi [49].

For Pr^{3+} a configurational coordinate diagram is shown in Fig. 3b. The $4f^1 5d$ level can lie above or below the $4f^2[^1S_0]$ level at about 47,000 cm^{-1}. In compounds where the $4f^1 5d$ level lies below the $4f^2[^1S_0]$ level, the energy gap between the $4f^1 5d$ level and the lower lying $4f^2[^3P_J]$ and $[^1I_6]$ levels is too large for non-radiative relaxation processes to be efficient and therefore $4f^1 5d \rightarrow 4f^2$ emission is observed. Compounds in which the $4f^1 5d$ level lies above the $4f^2[^1S_0]$ level show exclusively $4f^2 \rightarrow 4f^2$ line emission [50]. In compounds such as $LiLaP_4O_{12}$ and $LaPO_4$, Pr^{3+} only shows line emission at cryogenic temperatures and $4f^1 5d \rightarrow 4f^2$ emission appears upon increase of temperature [51,52]. In for example LaF_3, YF_3 and $SrAl_{12}O_{19}$, emission from the $4f^2[^1S_0]$ level can also be observed at room temperature [53–55]. Emission from the $4f^2[^1S_0]$ level can leave Pr^{3+} in the $4f^2[^1I_6]$ state [56], after which emission can subsequently take place from the $4f^2[^3P_0]$ state. Because of this, many Pr^{3+} compounds that show $4f^2[^1S_0]$ emission have been researched for their photon cascade emission, where two photons in the visible part of the spectrum are emitted after absorption of a single UV photon [57–59]. Compounds in which Pr^{3+} shows $4f^1 5d \rightarrow 4f^2$ emission at room temperature have been heavily researched for scintillation due to their exceptionally fast decay time of between 10 ns and 20 ns [60–62]. An overview of Pr^{3+}-doped compounds, their characteristics depending on the energy of the $4f^1 5d$ level relative to the $4f^2[^1S_0]$ level, and their application can be found in the works of Srivastava [63].

In this work, data on Sm^{2+} and Eu^{2+}-doped compounds showing $4f^{n-1}5d \rightarrow 4f^n$ emission are compiled to show the relation between emission wavelength and decay time. This relation is compared to a model of a three level system assuming a Boltzmann equilibrium between the populations of the $4f^{n-1}5d$ and excited $4f^n$ levels. The results are used to explain the large variation in Sm^{2+} $4f^5 5d \rightarrow 4f^6$ decay times reported in literature. The model is also used to predict the temperature dependence of this decay time as a function of $4f^5 5d \rightarrow 4f^6$ emission wavelength and the outcome is compared to the experimental data. The applicability of this model to development of new luminescence thermometers is discussed and new constraints are formulated to predict whether a Sm^{2+}-doped compound is a potential candidate for near-infrared scintillator applications. Lastly, an attempt has been made to predict the $4f^1 5d \rightarrow 4f^2$ decay time of Pr^{3+}-doped compounds.

2. Theory

When the population of the Sm^{2+} $4f^5 5d$ and $4f^6[^5D_0]$ levels are in thermal equilibrium, the ratio between the total number of ions in these respective states, N_{5d} and N_{4f}, can be expressed according to a Boltzmann distribution:

$$\frac{N_{4f}(t,T,\Delta E)}{N_{5d}(t,T,\Delta E)} = \frac{g_{4f}}{g_{5d}} e^{\frac{\Delta E}{kT}} \tag{3}$$

Here, $\Delta E = E_{5d} - E_{4f}$, which is the energy difference between the respective $4f^5 5d$ and $4f^6[^5D_0]$ states. g_{5d} and g_{4f} are their respective degeneracies. While N_{5d} and N_{4f} depend on time due to radiative decay, the ratio between them is independent of time as excited Sm^{2+} ions rapidly alternate between the two excited states. As the degeneracy of the excited states can vary from compound to compound and is generally unknown, it is assumed that $\frac{g_{4f}}{g_{5d}} = 1$ in the rest of this work.

Fig. 4 schematically shows how ΔE is determined in this work. The parabolas represent the electronic states of Sm^{2+} similar to the configurational coordinate diagram in Fig. 1, but this time only the three states taken into account within this model are drawn. The arrows indicate the relevant energy differences within the diagram. E_{4f} is the energy difference between the $4f^6[^7F_0]$ and $4f^6[^5D_0]$ states, which is found from the emission wavelength of the $4f^6[^5D_0] \rightarrow 4f^6[^7F_0]$ emission line λ_{4f} according to:

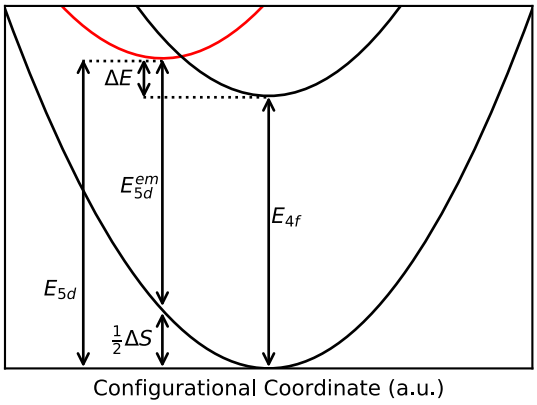

Fig. 4. Configurational coordinate diagram showing how the energy difference between the $4f^5 5d$ and $4f^6[^5D_0]$ states $\Delta E \equiv E_{5d} - E_{4f}$ is calculated from the transition energies E_{4f} and E_{5d}^{em} and the Stokes shift ΔS.

$$E_{4f} = \frac{hc}{\lambda_{4f}} \tag{4}$$

where h is the Planck constant and c the speed of light. Within this work, we will use λ_{4f} = 687 nm (14550 cm^{-1}) for all compounds. Following Fig. 4, E_{5d} is given by Equation (5):

$$E_{5d} = E_{5d}^{em} + \frac{1}{2}\Delta S = \frac{hc}{\lambda_{5d}} + \frac{1}{2}\Delta S \tag{5}$$

Here, E_{5d}^{em} is the energy of the $4f^5 5d \rightarrow 4f^6$ transition, which can be found from its emission wavelength λ_{5d}. ΔS is the Stokes shift between absorption and emission. Most compounds in which λ_{5d} of Sm^{2+} is close to 687 nm are iodides or bromides. On average, ΔS in these compounds is approximately 2000 cm^{-1} [64] and will be assumed that value in all other compounds as well.

Thermal equilibrium implies that phonon mediated transitions between the $4f^5 5d$ and $4f^6[^5D_0]$ levels are much faster than radiative decay to the ground state. In that case, the excited state of a single Sm^{2+} ion can be described as having a probability p_{5d} of being in the $4f^5 5d$ state and p_{4f} of being in the $4f^6[^5D_0]$ state, according to Equations (6) and (7):

$$p_{5d}(T,\Delta E) = \frac{N_{5d}}{N_{5d}+N_{4f}} = \frac{1}{e^{\frac{\Delta E}{kT}}+1} \tag{6}$$

$$p_{4f}(T,\Delta E) = \frac{N_{4f}}{N_{5d}+N_{4f}} = \frac{1}{e^{\frac{-\Delta E}{kT}}+1} \tag{7}$$

When two levels are not in thermal equilibrium, they both decay with their own intrinsic radiative lifetime. These are labelled τ_{5d} and τ_{4f} for the $4f^5 5d$ and $4f^6[^5D_0]$ levels, respectively. When they are in thermal equilibrium, they both show single exponential decay with the same decay time constant. In that case, the decay time can be found by a weighted average of τ_{5d} and τ_{4f}, where the weights are given by p_{5d} and p_{4f}:

$$\frac{1}{\tau(T,\Delta E)} = \frac{p_{5d}}{\tau_{5d}} + \frac{p_{4f}}{\tau_{4f}} \tag{8}$$

τ_{4f} is approximated to be 1 ms for all compounds. It is assumed that $\tau_{5d} \propto \lambda^3$ as predicted by the standard theory on luminescence decay [65] and based on the available decay time data at wavelengths longer than 750 nm it is approximated to be 3 μs at 850 nm [18,66–68]. τ_{5d} is then found by Equation (9):

Table 1
Input parameters for the model describing the $4f^{n-1}5d \rightarrow 4f^n$ decay times for Sm^{2+}, Eu^{2+} and Pr^{3+}.

Lanthanide	λ_{4f} (nm)	ΔS (cm^{-1})	τ_{4f} (μs)	τ_{5d} (μs)
Sm^{2+}	687	2000	1000	$3\left(\frac{\lambda_{5d}}{850\ nm}\right)^3$
Eu^{2+}	360	3000	1000	$0.5\left(\frac{\lambda_{5d}}{450\ nm}\right)^3$
Pr^{3+}	213	4000	1	$0.015\left(\frac{\lambda_{5d}}{230\ nm}\right)^3$

$$\tau_{5d} = 3\left(\frac{\lambda_{5d}}{850\ nm}\right)^3 \mu s \quad (9)$$

Equation (10) is found when combining Equations (6)-(8). This equation is identical to Equation (2), the one found by Feofilov and Tolstoi [32], except for omission of the terms describing the degeneracy of the states. This shows that both their model and the one described in this work are the same.

$$\tau(T,\Delta E) = \frac{1 + e^{\frac{-\Delta E}{kT}}}{\tau_{4f}^{-1} + \tau_{5d}^{-1} e^{\frac{-\Delta E}{kT}}} \quad (10)$$

Depending on the ratio between p_{5d} and p_{4f}, emission can be observed from both excited states. The luminescence intensity ratio between the $4f^5 5d \rightarrow 4f^6$ and $4f^6 \rightarrow 4f^6$ emission intensities (I_{5d} and I_{4f}) can be found using Equation (3), τ_{4f} and τ_{5d} and is expressed as:

$$\frac{I_{4f}}{I_{5d}} = \frac{\tau_{5d}}{\tau_{4f}} e^{\frac{\Delta E}{kT}} = \frac{\tau_{5d}}{\tau_{4f}} \frac{p_{4f}}{p_{5d}} \quad (11)$$

The same model applies for Eu^{2+} and Pr^{3+}, but different input parameters are required. For Eu^{2+}, λ_{4f} corresponds to the $4f^7[^6P_{7/2}] \rightarrow 4f^7[^8S_{7/2}]$ transition and a value of 360 nm (27800 cm^{-1}) is used [44]. The $4f^7 \rightarrow 4f^7$ emission is mostly observed in oxides and fluorides. ΔS of the $4f^6 5d \rightarrow 4f^7$ emission in these compounds is typically larger than in the bromides and iodides for which the Stokes shift of the Sm^{2+} $4f^5 5d \rightarrow 4f^6$ emission was estimated. Therefore, ΔS was determined to be on average 3000 cm^{-1} [64]. Just like for Sm^{2+}, τ_{4f} was taken to be 1 ms [44] and τ_{5d} was assumed to be 0.5 μs at 450 nm.

In the case of Pr^{3+}, a value of λ_{4f} = 213 nm (46900 cm^{-1}) applies for the $4f^2[^1S_0] \rightarrow 4f^2[^3H_4]$ transition [69]. Similar to Eu^{2+}, emission from the $4f^2[^1S_0]$ is also typically observed in fluorides and oxides, but ΔS for Pr^{3+} is larger than for Eu^{2+} [70], so an average ΔS of 4000 cm^{-1} is used [63,71]. The transitions from the $4f^2[^1S_0]$ state of Pr^{3+} are typically much faster than the $4f^n \rightarrow 4f^n$ transitions of Eu^{2+} and Sm^{2+}, so the value of τ_{4f} was taken to be 1 μs [53–55]. The approximated value for τ_{5d} is 15 ns at 230 nm [65]. The input parameters for the model of all lanthanides are summarised in Table 1.

3. Experimental techniques

$YbCl_2$:1%Sm^{2+} crystals were grown from the melt of binary starting materials in a Ta ampoule, as previously described in [67]. The growth of $CsBa_2I_5$:0.5%Sm^{2+} crystals in a silica ampoule was previously described in [18,66]. Cs_4EuI_6:0.5%Sm^{2+} crystals were grown from the melt in a Ta ampoule, as previously described in [68]. YbFBr:1%Sm^{2+} was synthesized from YbF_3, $YbBr_2$, $SmBr_2$, and Yb. YbF_3 was prepared from Yb_2O_3 (Metall Rare Earth Ltd., 6 N) and concentrated HF acid (Merck, suprapur, 40%). The oxide was reacted with HF acid in a Teflon beaker, dried on a sand bath, and treated by an Ar and HF gas stream in a glassy carbon boat at 450 °C inside an alloy 600 apparatus for fluorination and removal of oxygen traces. $YbBr_3$ and $SmBr_3$ were prepared from the oxides (Sm_2O_3, Fluka, 3 N) via the NH_4Br synthetic route [72] and sublimed under high vacuum in a silica apparatus for removal of oxygen impurities, as previously described, e.g., in [67]. The trihalides were reduced with the respective metal (Sm, Yb, Alfa, 3 N) in a Ta ampoule to obtain the dihalides $YbBr_2$ and $SmBr_2$. Ta ampoules were sealed by He-arc welding and protected in silica ampoules under vacuum. Stoichiometric amounts of YbF_3, $YbBr_2$, $SmBr_2$, and a small excess of Yb were sealed in a Ta ampoule, heated to 1080 °C, and slowly cooled by 3 K/h to 700 °C and 6 K/h to room temperature. All handling of starting materials and products was done in glove boxes or sealed sample containers under strictly dry and oxygen-free conditions.

For photoluminescence emission spectra, the sample was excited using a 450 W Xenon lamp in combination with a Horiba Gemini 180 monochromator. Quartz glass ampoules containing the samples under He gas were mounted directly on the cold finger of a Janis He cryostat and placed in a sample chamber. A Lakeshore Model 331 temperature controller was used to change the sample temperature. Emission light from the sample passed through an optical filter to block the excitation light before entering an optical fibre connected to an Ocean Insight QEPro spectrometer. The resulting spectra were corrected for the transmission of the optical fibre and sensitivity of the spectrometer.

Photoluminescence decay curves were measured using an EKSPLA NT230 OPO laser as excitation source with a repetition rate of 100 Hz and pulse duration of 10 ns. The temperature of the samples was controlled in an identical way as for the photoluminescence emission spectra. The emission light from the sample passed through an optical filter, after which it was detected using a SpectraPro-SP2358 monochromator and a Hamamatsu R7600U-20 PMT. The signal from the PMT was converted to a digital signal using a CAEN DT5724F digitizer.

4. Results

To illustrate the complex temperature dependence of Sm^{2+} emission, the photoluminescence emission and decay of two seemingly similar compounds are compared. The first compound is $YbCl_2$:1%Sm^{2+}. Its photoluminescence emission spectra between 10 K and 300 K at an excitation wavelength of 500 nm are shown in Fig. 5a. At 10 K, $YbCl_2$:1%Sm^{2+} shows $4f^6 \rightarrow 4f^6$ line emission on top of broad band $4f^5 5d \rightarrow 4f^6$ emission. Upon increasing the temperature to 100 K, the $4f^6 \rightarrow 4f^6$ lines gradually disappear. From 100 K onwards, $4f^6 \rightarrow 4f^6$ lines are no longer visible and the emission spectrum only contains the $4f^5 5d \rightarrow 4f^6$ broad band emission. The maximum of the $4f^5 5d \rightarrow 4f^6$ emission band shows a small shift to longer wavelengths as temperature increases and is 727 nm at 300 K. This results in a value of ΔE = 200 cm^{-1}, meaning the $4f^5 5d$ state lies just above the $4f^6[^5D_0]$ state.

The decay curves of the $4f^5 5d \rightarrow 4f^6$ emission monitored at 720 nm are shown in Fig. 5b. At 10 K, the emission consists of a decay component too fast for the response time of the setup (10 ns) and a slow component with a decay time of 430 μs. A fast and slow component with similar decay times were also observed in BaBrI:Sm^{2+} by Sofich et al. and in $BaCl_2$:Sm^{2+} by He et al. (ΔE = 1460 cm^{-1} and ΔE = 1710 cm^{-1}) [73,74]. He et al. ascribed the slow component to thermal repopulation of the $4f^5 5d$ state from the $4f^6[^5D_0]$ state, as both the $4f^5 5d \rightarrow 4f^6$ and the $4f^6 \rightarrow 4f^6$ had the same decay time. The fast component is much faster than the intrinsic decay time of the Sm^{2+} emission, indicating the decay is accelerated by out-of-equilibrium processes, as discussed below in Section 5. As ΔE is positive, the fast decay is ascribed to $4f^5 5d \rightarrow 4f^6$ emission in the out-of-equilibrium situation. Rapid thermal relaxation to the lower lying $4f^6[^5D_0]$ state eventually leads to the Boltzmann distribution with long decay time. Upon increasing the temperature, the intensity of the fast component decreases until it is no longer visible at 100 K, the same temperature at which the $4f^6 \rightarrow 4f^6$ lines disappear in the emission spectrum in Fig. 5a. Simultaneously, the decay time of the slow component steadily decreases, indicating that the rate of thermal repopulation from $4f^6[^5D_0]$ to $4f^5 5d$ increases with temperature.

The decay time constants of the $4f^5 5d \rightarrow 4f^6$ emission as a function of temperature are shown in Fig. 5c. For temperatures between 10 K and 100 K, only the decay time values of the slow component are included. It shows that at 100 K, the lowest temperature at which only $4f^5 5d \rightarrow 4f^6$ emission is visible in the emission spectrum, the decay time is still shortening rapidly. A further increase in temperature to 500 K further shortens the decay time by almost an order of magnitude after which it stabilises. Around 700 K, another decrease in decay time associated

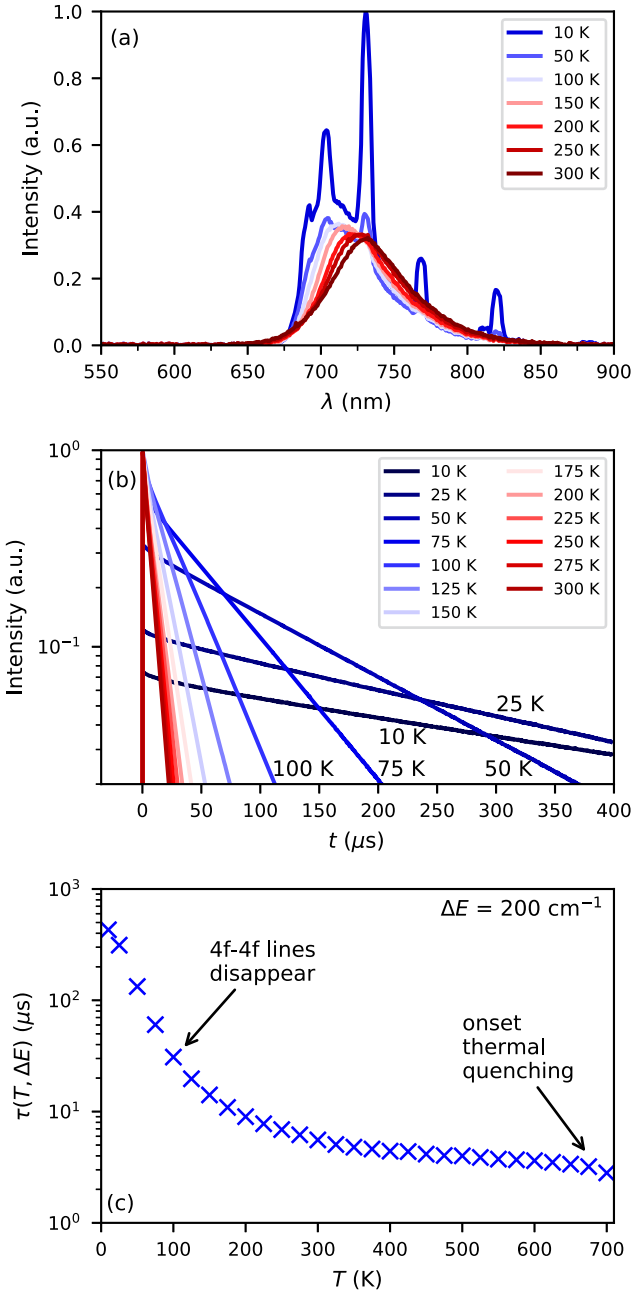

Fig. 5. $YbCl_2$:1%Sm^{2+} excited at 500 nm into the $4f^55d$ state, a) Photoluminescence emission spectra, b) Photoluminescence decay curves monitored at 720 nm, and c) Decay times of Sm^{2+} emission versus temperature.

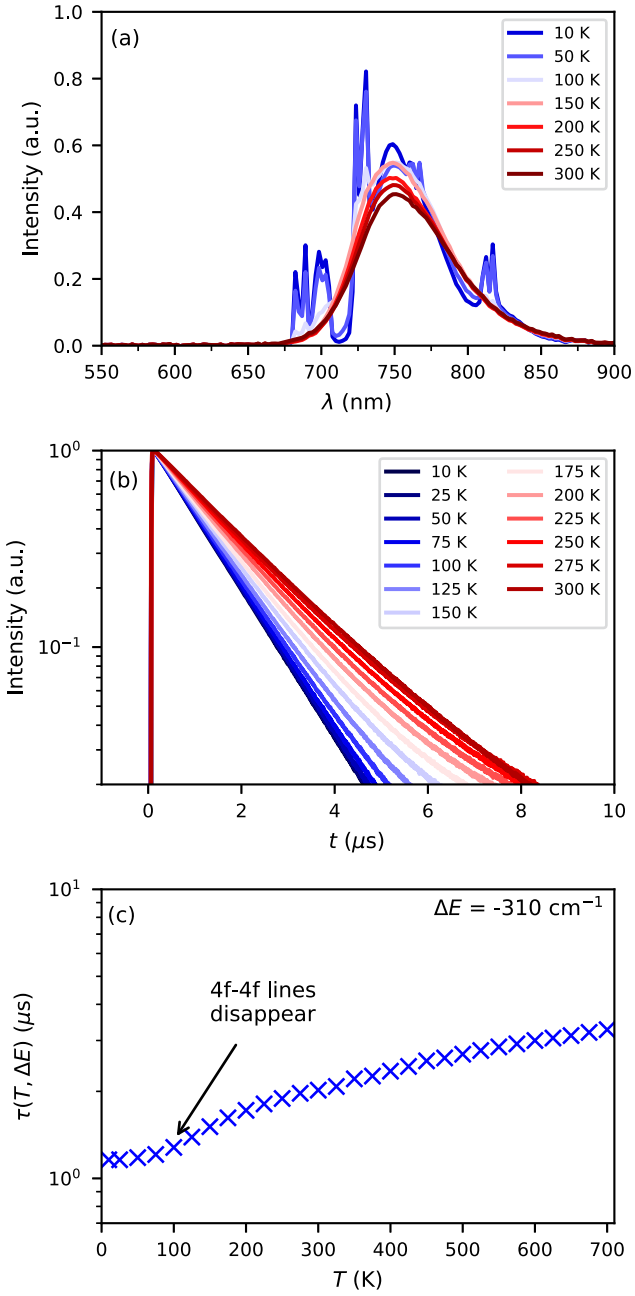

Fig. 6. $CsBa_2I_5$:0.5%Sm^{2+} excited at 500 nm into the $4f^55d$ state, a) Photoluminescence emission spectra, b) Photoluminescence decay curves monitored at 750 nm, and c) Decay times of Sm^{2+} emission versus temperature.

with the onset of thermal quenching is observed. These results show that when an emission spectrum at room temperature contains exclusively $4f^55d \rightarrow 4f^6$ emission, the rate of thermal repopulation from the $4f^6[^5D_0]$ state can still lengthen the decay time observed for the $4f^55d \rightarrow 4f^6$ emission. Similar temperature dependence of the decay time was previously observed in $SrCl_2$:Sm^{2+} and $SrBr_2$:Sm^{2+} [35].

The second example is $CsBa_2I_5$:0.5%Sm^{2+}. Fig. 6a shows the photoluminescence emission spectra between 10 K and 300 K excited at 500 nm. Similar to the photoluminescence emission spectra of $YbCl_2$:1%Sm^{2+}, the 10 K emission spectrum shows $4f^6 \rightarrow 4f^6$ line emission on top of broad band $4f^55d \rightarrow 4f^6$ emission. The $4f^6 \rightarrow 4f^6$ line emission intensity again decreases upon increase of temperature and from 100 K onwards, exclusively $4f^55d \rightarrow 4f^6$ emission is visible in the emission spectrum. The temperature dependence of the emission spectra shows no large difference between $YbCl_2$:1%Sm^{2+} and $CsBa_2I_5$:0.5%Sm^{2+}, however the emission band maximum of $\lambda_{5d} = 755$ nm implies with Equation (5) that $\Delta E = -310$ cm^{-1}, which means that the $4f^55d$ level now lies below the $4f^6[^5D_0]$ level.

Fig. 6b shows the corresponding decay curves of the $4f^55d \rightarrow 4f^6$ emission, excited at 500 nm and monitored at 750 nm. As opposed to rapid shortening of the decay time with increasing temperature that was seen in $YbCl_2$:1%Sm, the Sm^{2+} emission in $CsBa_2I_5$:0.5%Sm^{2+} gradually lengthens as temperature is increased. Apparently the change of sign of ΔE can cause an extreme difference in the decay dynamics that is not necessarily manifest in the photoluminescence emission spectra of the two samples. Fig. 6c shows the decay time constants of the $4f^55d \rightarrow 4f^6$ emission as a function of temperature. The temperature at which the $4f^6 \rightarrow 4f^6$ emission lines disappear coincides with the temperature at which the decay time starts to lengthen.

Table 2
Room temperature decay times $\tau(300\,\mathrm{K}, \Delta E)$ of Sm^{2+} $4f^55d \rightarrow 4f^6$ emission in various compounds. λ_{5d} denotes the wavelength of the $4f^55d \rightarrow 4f^6$ emission band maximum and $\Delta E = E_{5d} - E_{4f}$ in the configurational coordinate diagram.

Compound	λ_{5d} (nm)	ΔE (cm^{-1})	$\tau(300\,\mathrm{K}, \Delta E)$ (μs)	ref.
$BaCl_2$	655	1710	1700	[74]
$BaCl_2$:12.5%La	655	1710	100	[75]
KY_3F_{10}	660	1600	230	[76]
$Sm(AlCl_4)_2$	660	1600	275	[31]
YbFBr	662	1550	409	This work
BaBrI	666	1460	2150	[73]
BaFI	675	1260	350	[77,78]
$Sr_{0.7}Ba_{0.3}Cl_2$	680	1150	15	[79]
$SrCl_2$	690	940	13	[35]
CsBr	695	830	15	[80]
$SrBr_2$	702	690	13	[35]
$Sm(AlBr_4)_2$	712	490	35	[31]
$KSrPO_4$	715	430	390	[81]
$YbCl_2$	727	200	5.2	[67]
KCl	730	140	4.3	[20]
SrI_2	740	43	1.5	[17,30,35]
$CsBa_2I_5$	755	-310	2.1	[18,66]
$CsYbBr_3$	780	-740	2.1	[67]
$CsYbI_3$	800	-1060	2.3	[67]
Cs_4EuBr_6	820	-1360	3.5	[68]
Cs_4EuI_6	848	-1760	3.5	[68]

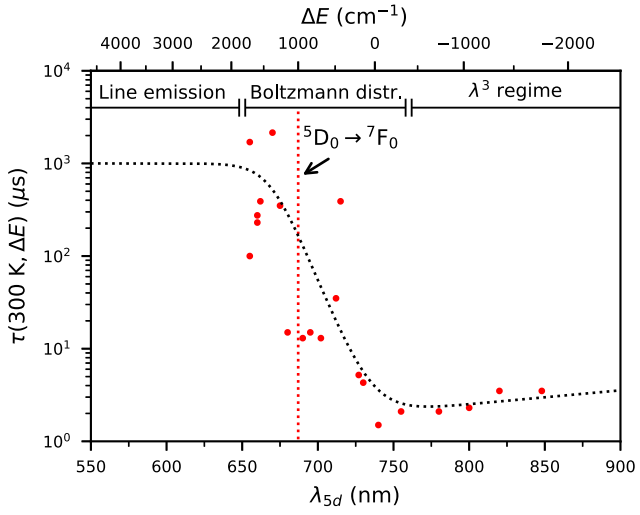

Fig. 7. Room temperature decay times of Sm^{2+} $4f^55d \rightarrow 4f^6$ emission in various compounds. The red dashed line indicates the energy of the $4f^6[^5D_0] \rightarrow 4f^6[^7F_0]$ transition.

To further investigate the interplay between the $4f^55d$ and $4f^6[^5D_0]$ levels, data on $\tau(300\,\mathrm{K}, \Delta E)$ measured on the Sm^{2+} $4f^55d \rightarrow 4f^6$ emission in various compounds have been compiled in Table 2. A plot of $\tau(300\,\mathrm{K}, \Delta E)$ versus λ_{5d} is shown in Fig. 7. ΔE is negative for $\lambda_{5d} >$ 740 nm. In this wavelength range the data points are well described by a λ_{5d}^3 trend line. At $\lambda_{5d} <$ 740 nm, where ΔE is positive, the λ_{5d}^3 trend is broken and τ starts to rapidly increase.

The calculated values of $\tau(300\,\mathrm{K}, \Delta E)$ using Equation (10) are shown by the black dotted line in Fig. 7. The model follows the data well and accurately predicts that $\tau(300\,\mathrm{K}, \Delta E)$ increases when $\lambda_{5d} <$ 740 nm and also the steepness of this increase corresponds well to the data. It also explains why no data points were found for $\lambda_{5d} <$ 650 nm, as this is where $\tau(300\,\mathrm{K}, \Delta E)$ converges to the 1 ms value of τ_{4f}, and then following Equations (10) and (11) those compounds show exclusively $4f^6 \rightarrow 4f^6$ emission.

To further explore the different types of temperature behaviour of $\tau(T, \Delta E)$, 4 compounds with different ΔE are analysed in Fig. 8. Fig. 8a shows the configurational coordinate diagram of Sm^{2+} in 4 different

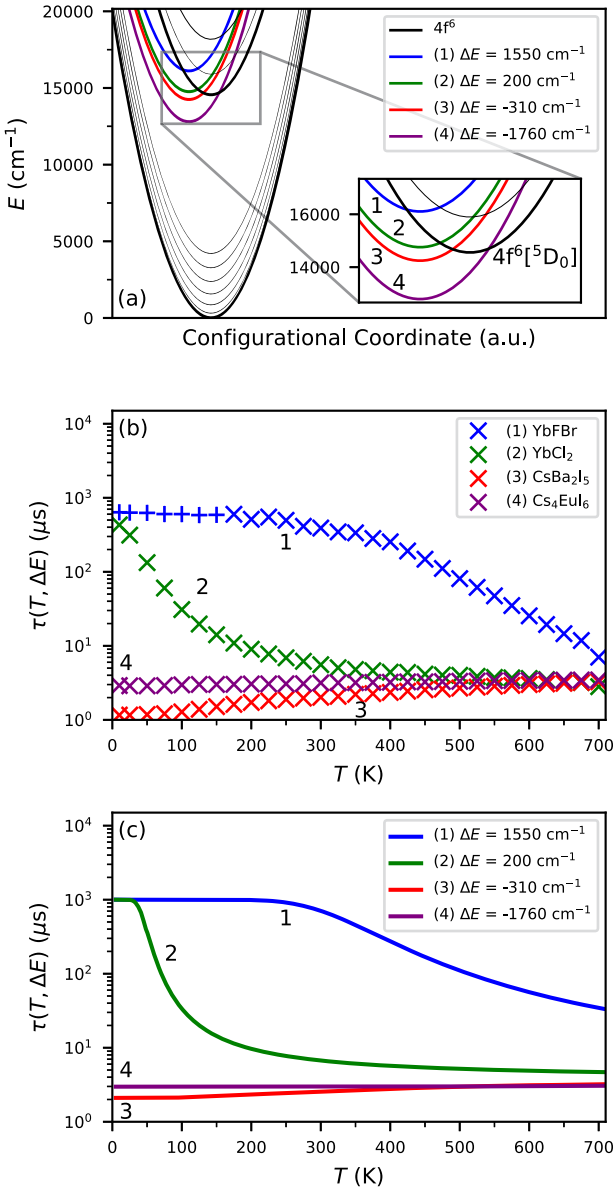

Fig. 8. Decay times of Sm^{2+} $4f^55d \rightarrow 4f^6$ emission as a function of temperature. a) The configurational coordinate diagrams show the energy difference between the $4f^55d$ and $4f^6[^5D_0]$ levels for all four compounds. b) Experimentally observed temperature dependence of $\tau(T, \Delta E)$. Datapoints marked with "+" indicate $4f^6 \rightarrow 4f^6$ decay times. c) The calculated temperature dependence of $\tau(T, \Delta E)$.

compounds. The black parabolas represent the $4f^6$ states and are the same for all compounds. Parabola 1 represents the $4f^55d$ state for λ_{5d} = 662 nm (ΔE = 1550 cm^{-1}), which corresponds to YbFBr:1%Sm^{2+}. Parabola 2 corresponds to λ_{5d} = 727 nm (ΔE = 200 cm^{-1}), which is the case for $YbCl_2$:1%Sm^{2+}. Parabola 3 has λ_{5d} = 755 nm (ΔE = −310 cm^{-1}), corresponding to $CsBa_2I_5$:0.5%Sm^{2+}. Lastly, parabola 4 represents the situation for λ_{5d} = 848 nm (ΔE = −1760 cm^{-1}), which is the case for Cs_4EuI_6:0.5%Sm^{2+}.

The experimental values of $\tau(T, \Delta E)$ as a function of temperature for these 4 compounds are shown in Fig. 8b. Curve 1 shows the experimental data for YbFBr:1%Sm^{2+}. Below 175 K, $\tau(T, 1550\ cm^{-1})$ could not be accurately determined by measuring the $4f^55d \rightarrow 4f^6$ emission as its intensity was too low. Therefore, data points between 10 K and 150 K were determined from the $4f^6 \rightarrow 4f^6$ emission decay time. The data points at 150 K and 175 K have approximately the same value, which confirms that $\tau(T, 1550\ cm^{-1})$ is the same for both the $4f^55d \rightarrow$

$4f^6$ and $4f^6 \rightarrow 4f^6$ emission. $\tau(T, 1550\ cm^{-1})$ remains almost constant until 350 K, after which it starts to gradually decrease. This means that up to 300 K, the emission spectrum mostly consists of $4f^6 \rightarrow 4f^6$ lines, as was also observed by Schipper and Blasse [82].

Curve 2 shows the experimental data for $YbCl_2$:1%Sm^{2+} (ΔE = 200 cm^{-1}), which are the same as shown in Fig. 5c. Opposed to YbFBr:1%Sm^{2+}, $\tau(T, 200\ cm^{-1})$ of $YbCl_2$:1%Sm^{2+} starts to decrease already from 10 K onwards and converges to around 3.5 μs at 500 K. Curve 3 shows $\tau(T, -310\ cm^{-1})$ for $CsBa_2I_5$:0.5%Sm^{2+}, which are the same as shown in Fig. 6c, and shows the steady increase in $\tau(T, -310\ cm^{-1})$ from 1.2 μs at 10 K to 3.2 μs at 700 K. Lastly, Curve 4 shows the experimental data for Cs_4EuI_6:0.5%Sm^{2+}. Its value for $\tau(T, -1760\ cm^{-1})$ slowly increases from 2.9 μs to 3.4 μs from 10 K to 700 K. Its value at 10 K is higher than that of $CsBa_2I_5$:0.5%Sm^{2+} and it has a smaller temperature dependence.

The calculated temperature behaviour of $\tau(T, \Delta E)$ for all 4 compounds is shown in Fig. 8c. Curve 1 corresponds to ΔE = 1550 cm^{-1} (YbFBr:1%Sm^{2+}). $\tau(T, 1550\ cm^{-1})$ is stable at 1 ms from 0 K until almost 300 K. This value of 1 ms corresponds to τ_{4f} set in the model and means thermal population from the $4f^6[^5D_0]$ to the $4f^5$5d state is extremely unlikely and even when it occurs, thermal relaxation back down to the $4f^6[^5D_0]$ state will be much faster than emission. Above 300 K, $\tau(T, 1550\ cm^{-1})$ starts to decrease as there is enough thermal energy to excite Sm^{2+} from the $4f^6[^5D_0]$ to the $4f^5$5d state. The temperature at which this occurs agrees reasonably well with the experimental data in Fig. 8b. $\tau(T, 1550\ cm^{-1})$ decreases less in the calculated data than in the experimental data. This may be caused by the close lying $4f^6[^5D_1]$ level in combination with the onset of thermal quenching, which can for example be seen by the more rapid downturn in the final step from 675 K to 700 K in the experimental data.

Curve 2 corresponds to ΔE = 200 cm^{-1} ($YbCl_2$:1%Sm^{2+}). Its behaviour is similar to Curve 1, where $\tau(T, 200\ cm^{-1})$ is first 1 ms over an initial temperature range and then rapidly decreases as enough thermal energy becomes available to excite Sm^{2+} from the $4f^6[^5D_0]$ to the $4f^5$5d state. However, as ΔE is almost 8 times smaller than for Curve 1, all changes happen at 8 times lower temperature. This can be understood from Equation (10), in which the exponent in the denominator is responsible for most of the temperature dependence. A ΔE that is 8 times smaller requires an 8 times lower temperature for the same change in $\tau(T, \Delta E)$. As a result, the range in which $\tau(T, 200\ cm^{-1})$ is stable at 1 ms stops well below 50 K, shortly after which the $4f^6 \rightarrow 4f^6$ lines disappear from the emission spectrum in Fig. 5a. The subsequent decrease in $\tau(T, 200\ cm^{-1})$ is also 8 times as steep compared to $\tau(T, 1550\ cm^{-1})$. This calculated data accurately explains that the difference between the temperature dependence of $\tau(T, \Delta E)$ of YbFBr:1%Sm^{2+} and $YbCl_2$:1%Sm^{2+} is primarily driven by their difference in ΔE.

Curve 3 shows the calculated temperature behaviour for ΔE = −310 cm^{-1} ($CsBa_2I_5$:0.5%Sm^{2+}). As ΔE is now negative, the $4f^5$5d state will be preferentially occupied at low temperatures and therefore $\tau(T, -310\ cm^{-1}) = \tau_{5d}$ at 0 K, almost 3 orders of magnitude faster than for Curves 1 and 2. Upon increase of the temperature, $\tau(T, -310\ cm^{-1})$ becomes longer as the $4f^6[^5D_0]$ state starts to become populated, similar to what is observed in the experimental data on $CsBa_2I_5$:0.5%Sm^{2+} (Fig. 8b). This means that lengthening of $\tau(T, -310\ cm^{-1})$ with increasing temperature is an intrinsic property of Sm^{2+} when ΔE is negative and has a small magnitude. At 10 K, a value of $\tau(T, -310\ cm^{-1})$ is around 2 μs for the calculated curve, while the experimental data on $CsBa_2I_5$:0.5%Sm^{2+} show 1.2 μs at 10 K, meaning τ_{5d} has been estimated too high for this compound. $\tau(T, -310\ cm^{-1})$ increases with temperature and reaches a value of 3.2 μs at 700 K, indicating the $4f^6[^5D_0]$ state becomes more populated.

Finally, Curve 4 shows the situation for $\Delta E = -1760\ cm^{-1}$ (Cs_4EuI_6: 0.5%Sm^{2+}). At 0 K, $\tau(T, -1760\ cm^{-1})$ is significantly longer than for Curve 3. This is caused by the λ_{5d}^3 dependence of τ_{5d}. This is also observed in the experimental data in Fig. 8b. As ΔE is almost 6 times as large as for Curve 3, the change in $\tau(T, -1760\ cm^{-1})$ is again spread out over a 6 times larger temperature range than $\tau(T, -310\ cm^{-1})$. The result is that $\tau(T, -1760\ cm^{-1})$ seems almost independent of temperature. This is also in line with the experimental data, where the smallest temperature dependence of $\tau(T, \Delta E)$ of all samples is found in Cs_4EuI_6:0.5%Sm^{2+}.

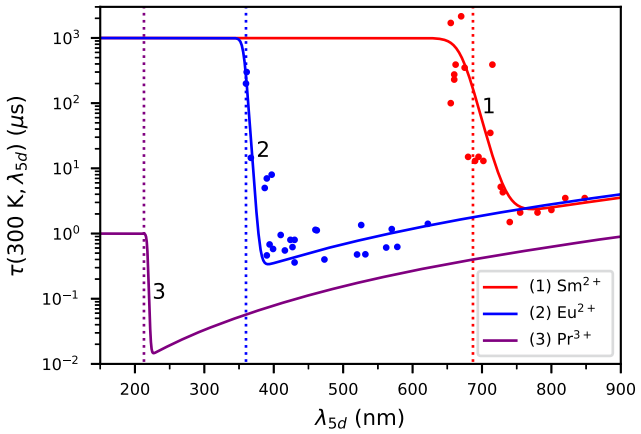

Fig. 9. Room temperature decay times of $4f^{n-1}5d \rightarrow 4f^n$ emission of (1) Sm^{2+}, (2) Eu^{2+}, and (3) Pr^{3+} against wavelength.

Table 3
Room temperature decay times $\tau(300\ K, \Delta E)$ of Eu^{2+} $4f^6$5d → $4f^7$ emission in various compounds. λ_{5d} denotes the wavelength of the $4f^6$5d → $4f^7$ emission band maximum and $\Delta E = E_{5d} - E_{4f}$ in the configurational coordinate diagram.

Compound	λ_{5d} (nm)	ΔE (cm^{-1})	$\tau(300\ K, \Delta E)$ (μs)	ref.
$SrAlF_5$	360	1500	200	[44]
$LiBaAlF_6$	361	1420	300	[83]
SrB_4O_7	367	970	14.5	[84]
SrFCl	387	-440	5.0	[85]
BaFCl	390	-640	7.0	[85]
$SrMgP_2O_7$	390	-640	0.46	[86]
BaFBr	394	-900	0.68	[45]
$SrAl_{12}O_{19}$	397	-1090	8	[48,87]
$BaCl_2$	399	-1220	0.58	[85]
$SrCl_2$	410	-1890	0.95	[85]
SrF_2	416	-2240	0.55	[85]
CaF_2	424	-2690	0.8	[85]
SrI_2	427	-2860	0.7	[88]
$CaCl_2$	430	-3020	0.8	[85]
$CsBa_2I_5$	430	-3020	0.36	[89]
Cs_4SrI_6	460	-4540	1.14	[90]
Cs_4CaI_6	462	-4630	1.12	[90]
$BaAl_2S_4$	473	-5140	0.4	[91]
$KLuS_2$	520	-7050	0.48	[92]
$CsCaF_3$	526	-7270	1.35	[93]
$SrGa_2S_4$	532	-7480	0.48	[94]
$CaGa_2S_4$	562	-8480	0.61	[95]
$LiSrSiO_4$	570	-8730	1.17	[96]
Sr_3SiO_5	578	-8980	0.63	[97]
$Rb_3YSi_2O_7$	622	-10200	1.41	[98]

The model has also been applied to Eu^{2+} and Pr^{3+} and its results are shown in Fig. 9. $\tau(300\ K, \Delta E)$ data measured on the Eu^{2+} $4f^6$5d → $4f^7$ emission have been collected. Only data were used in which the effects of thermal quenching, concentration quenching, and self-absorption were minimal. The $\tau(300\ K, \Delta E)$ values are shown in Table 3 and plotted against λ_{5d} in Fig. 9, together with those of Sm^{2+}. The calculated curves of $\tau(300\ K, \Delta E)$ for Sm^{2+} (Curve 1), Eu^{2+} (Curve 2), and Pr^{3+} (Curve 3) are also shown in Fig. 9, using the input parameters from Table 1.

For $\lambda_{5d} > 400$ nm the calculated values of $\tau(300\ K, \Delta E)$ for Eu^{2+} are primarily described by the λ^3 dependence of τ_{5d} and the Eu^{2+} data scatter nicely around it. When $\lambda_{5d} < 400$ nm, the calculated values show an increase in $\tau(300\ K, \Delta E)$ and converge to the value of 1

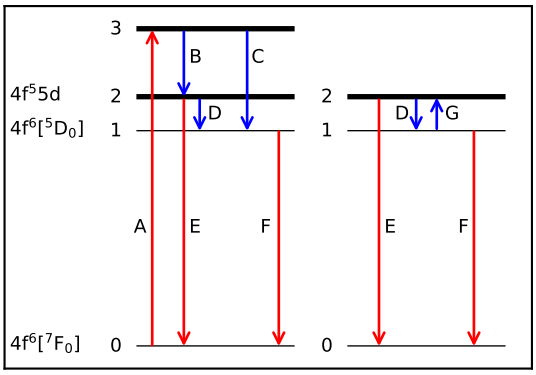

Fig. 10. Schematic showing the origin of the fast component in the luminescence decay of Sm^{2+}. Left: Directly after excitation an excess of $4f^5 5d$ excitations causes a fast component and Right: Situation after Boltzmann distribution between the $4f^5 5d$ and $4f^6[^5D_0]$ states is established.

ms that corresponds to τ_{4f} around 350 nm. The wavelength range in which $\tau(300\text{ K}, \Delta E)$ increases is more narrow than for Sm^{2+}, which is solely caused by the nonlinear conversion from an energy to wavelength scale. On an energy scale, both ranges would have equivalent size. In the wavelength range between 350 nm and 400 nm, some compounds show a longer $\tau(300\text{ K}, \Delta E)$ value than the typical decay times for τ_{5d} of between 0.5 μs and 1 μs. These data points follow the calculated increase in $\tau(300\text{ K}, \Delta E)$ well and thereby show that this model can be effectively applied to Eu^{2+}.

For Pr^{3+}, the resulting relation between $\tau(300\text{ K}, \Delta E)$ and λ_{5d} is shown by Curve 3 in Fig. 9. Unfortunately, no $\tau(300\text{ K}, \Delta E)$ data could be found that confirms that the model can be applied to Pr^{3+} as well. Data on Pr^{3+} $4f^1 5d \rightarrow 4f^2$ decay times near 225 nm are scarce, which is likely due to experimental difficulty as it requires measuring decay times of around 10 ns with a vacuum UV excitation source. The temperature dependent decay times of the Pr^{3+} $4f^2[^1S_0]$ state in $LaPO_4$ and $LiLaP_4O_{12}$ were reported by Srivastava et al. and show similar temperature dependence as the $4f^5 5d \rightarrow 4f^6$ emission of Sm^{2+} in $YbCl_2$ [51,52]. The compounds show respective emission wavelengths λ_{5d} of 228 nm and 217 nm and fall precisely within the wavelength range where the $\tau(300\text{ K}, \Delta E)$ increases. Unfortunately, no data on the room temperature decay times were presented and it cannot be verified that the two states are in thermal equilibrium.

5. Discussion

The described decay time model of Equation (10) only holds when the Sm^{2+} $4f^5 5d$ level and $4f^6[^5D_0]$ level are in thermal equilibrium. An example of an out-of-equilibrium situation is encountered in Fig. 5b, where the photoluminescence decay of $YbCl_2$:1%Sm^{2+} shows a <10 ns fast component between 10 K and 100 K in addition to the slow component that was visible at all temperatures. Only the origin of the slow component is described by the decay time model expressed by Equation (10). The origin of the fast component is illustrated by the left schematic of Fig. 10. Sm^{2+} is optically excited into one of the higher lying $4f^5 5d$ levels, corresponding to arrow A. After this, relaxation to the lower lying levels through arrows B and C will result in a distribution over the $4f^5 5d$ and $4f^6[^5D_0]$ levels that does not necessarily match the distribution that corresponds to Boltzmann statistics. Using Equation (7) with $\Delta E = 200$ cm^{-1} and $T = 100$ K, the Boltzmann distribution is established when $p_{4f} = 95\%$ and consequently $p_{5d} = 5\%$. It is therefore likely that the initial distribution contains an overpopulation of Sm^{2+} ions in the $4f^5 5d$ state.

Nonradiative decay to the $4f^6[^5D_0]$ state via arrow D with rate k_{21} and radiative decay to the ground state via arrow E with rate τ_{5d}^{-1} will make the excited Sm^{2+} population converge to the Boltzmann distribution. The fast component in Fig. 5b is then an indication of how fast the population converges to the Boltzmann distribution and its decay time τ_f is given by Equation (12).

$$\frac{1}{\tau_f} = \frac{1}{\tau_{5d}} + k_{21} \tag{12}$$

As τ_{5d} is approximately 2 μs and τ_f in Fig. 5b is <10 ns, k_{21} has by far the largest contribution to this decay time, even at 10 K. k_{21} is typically caused by the interconfigurational crossing of the $4f^5 5d$ and $4f^6[^5D_0]$ states and therefore the rate is expected to increase with temperature. As a consequence, the time it takes for the excitations to reach a Boltzmann distribution will become even shorter at higher temperatures until the fast component can no longer be observed.

After the fast component has disappeared, the Boltzmann distribution has been established and the schematic on the right of Fig. 10 applies. The electronic configuration of the Sm^{2+} ions is constantly switching between the $4f^5 5d$ and $4f^6[^5D_0]$ states through arrows D and G. At any point in time, the probability to find a Sm^{2+} ion in each of the two states now corresponds to p_{5d} in Equation (6) and p_{4f} in Equation (7). In this situation, radiative decay is possible from both excited states via arrows E and F. In $YbCl_2$:1%Sm^{2+} at 100 K however, where $p_{4f} = 95\%$ and $p_{5d} = 5\%$, the emission spectrum shows almost exclusively $4f^5 5d \rightarrow 4f^6$ emission. This can be understood from Equation (11). As τ_{5d} is roughly 500 times shorter than τ_{4f} for Sm^{2+}, Sm^{2+} ions will preferentially decay through the $4f^5 5d \rightarrow 4f^6$ transition and less than 4% of the total emission intensity comes from the $4f^6 \rightarrow 4f^6$ emission. At 300 K, this will even be less than 0.5%. When not specifically looking for the presence of $4f^6 \rightarrow 4f^6$ lines by employing spectroscopic techniques with high wavelength resolution and exceptional signal to noise ratio, these $4f^6 \rightarrow 4f^6$ lines will likely go unnoticed and only broad band $4f^5 5d \rightarrow 4f^6$ emission will be observed.

For luminescence thermometry, a large relative sensitivity S_r is acquired when $\tau(T, \Delta E)$ rapidly changes with temperature (see Equation (1)). It can be seen in Fig. 8 that the largest changes in $\tau(T, \Delta E)$ are found when ΔE is positive and its magnitude is small. It was for example recently found that doping SrB_4O_7 with Eu^{2+} for luminescent thermometer applications results in much higher S_r values than what is achieved with Sm^{2+}-doping in SrB_4O_7 [84]. One cause for this is that in SrB_4O_7, the ΔE between the $4f^7[^6P_{7/2}]$ and $4f^6 5d$ states of Eu^{2+} (130 cm^{-1} [99]) is almost 25 times smaller than ΔE between the $4f^6[^5D_0]$ and $4f^5 5d$ states of Sm^{2+} (3100 cm^{-1} [25]). This shifts the temperature at which S_r has its maximum value from roughly 550 K [26] to around 20 K [84], but simultaneously increases the maximum achievable S_r value by the same factor 25. Sójka et al. reported an S_r value of over 10% at 20 K in SrB_4O_7:Eu^{2+} [84], compared to the 3.3% at 550 K reported for SrB_4O_7:Sm^{2+} [26]. By monitoring the luminescence intensity ratio between the Eu^{2+} $4f^n \rightarrow 4f^n$ emission with that of Sm^{2+}, Zheng et al. achieved S_r values of over 40% at temperatures below 20 K [100]. This shows that the high S_r values at cryogenic temperatures are a direct consequence of a small ΔE.

Another small contribution to the larger S_r can be found in the shorter τ_{5d} of the Eu^{2+} $4f^{n-1}5d \rightarrow 4f^n$ emission compared to that of Sm^{2+}, which is primarily due to the shorter λ_{5d}. The total change in $\tau(T, \Delta E)$ is approximately the difference between τ_{4f} and τ_{5d}. This difference increases as τ_{5d} becomes smaller. A larger change in $\tau(T, \Delta E)$ in turn results in higher values of S_r, which means that Eu^{2+} should give larger values for S_r than Sm^{2+} when they have the same ΔE.

For scintillators there is a strong preference for materials with a short $\tau(300\text{ K}, \Delta E)$. Wolszczak et al. formulated a criterion for using Sm^{2+} as a dopant for scintillation saying that it must exclusively show $4f^5 5d \rightarrow 4f^6$ emission, resulting in a restriction of $\lambda_{5d} > 698$ nm [101]. From Fig. 7 it can be seen that this criterion should be formulated more strictly. The model presented in this work predicts that around $\lambda_{5d} =$ 700 nm, τ is already over an order of magnitude longer than it is at its minimum value around 750 nm. A better criterion would therefore be that λ_{5d} should be no shorter than 730 nm. Going to longer wavelengths than 750 nm, the decay time lengthens again due to the λ_{5d}^3

dependence. This lengthening is however much less severe and should not impose a restriction on what λ_{5d} can be used. Looking at Table 2, it can be seen that the criterion of $\lambda_{5d} > 730$ nm is often achieved in iodides (large nephelauxetic effect) or compounds in which Sm^{2+} sits on a site with octahedral symmetry (large crystal field splitting).

$\lambda_{5d} > 730$ nm implies that ideally ΔE is negative for scintillators. For negative ΔE, the $4f^6 \rightarrow 4f^6$ emission is often completely absent at all temperatures. An increase in temperature promotes Sm^{2+} to the slowly decaying $4f^6[^5D_0]$ level and thereby lengthens $\tau(T, \Delta E)$. This effect is most prominent when the magnitude of ΔE is small, as can be seen by the differences in curves 3 and 4 in Fig. 8. While lengthening of $\tau(T, \Delta E)$ is an intrinsic property of Sm^{2+} in compounds like $CsBa_2I_5$, it strongly resembles the effect of self-absorption. When Sm^{2+} emits a photon in the wavelength range where other Sm^{2+} ions can reabsorb it, there is a probability that the photon is reabsorbed before leaving the material. It then again takes time for the newly excited Sm^{2+} to emit a photon, lengthening the decay time and increasing the probability of luminescence quenching. This effect is detrimental for applications in which large crystals are required, as a photon travelling through the crystal encounters more Sm^{2+} ions before exiting the crystal, increasing the probability of self-absorption. Lengthening of the decay time with increasing temperature is often ascribed to self-absorption, as absorption and emission bands broaden and the overlap between them grows, increasing the probability that a photon is re-absorbed. With the knowledge that the lengthening of $\tau(T, \Delta E)$ with increasing temperature is an intrinsic property of Sm^{2+}, it is more reliable to probe the probability of self-absorption comparing samples of different sizes or Sm^{2+} concentrations, rather than relying on temperature dependent data.

Even though $\tau(300\ \mathrm{K}, \Delta E)$ values are suitable for scintillation for $\lambda_{5d} > 730$ nm, some additional restrictions on λ_{5d} might be imposed by the choice of photodetector. Silicon based photodetectors typically show optimal performance between 400 nm and 800 nm, where almost all undetected photons are reflected from the detector. These photons can be recovered by wrapping the scintillator and detector combination in reflective material, giving the photons a second chance to be detected [102]. At wavelengths longer than 800 nm, silicon starts to become transparent and transmission losses occur. Even detectors optimised for near-infrared detection show a sharp drop in quantum efficiency between 900 nm and 950 nm. When a significant part of the Sm^{2+} emission spectrum lies beyond 950 nm, the number of detected photons decreases, which worsens the energy resolution. The longest wavelength emitting scintillator in Table 2 is Cs_4EuI_6:Sm^{2+} with λ_{5d} = 848 nm [68]. The Sm^{2+} $4f^55d \rightarrow 4f^6$ emission in this compound shows a tail extending beyond 1000 nm, meaning losses already occur when coupling it to a silicon based photodetector. Losses are expected to be minimal for compounds with $\lambda_{5d} < 800$ nm. This means that the ideal λ_{5d} for near-infrared scintillators with silicon based photodetector read out sits in a narrow window from 730 nm to 800 nm. It is worth pointing out that the currently best performing NIR scintillator $CsBa_2I_5$:2%Eu^{2+},1%Sm^{2+} with its λ_{5d} of 755 nm lies within this window and even close to the minimum value of $\tau(300\ \mathrm{K}, \Delta E)$.

6. Conclusions

The effect of a Boltzmann distribution establishing between population of the Sm^{2+} $4f^55d$ and $4f^6[^5D_0]$ levels on $4f^55d \rightarrow 4f^6$ decay time has been modelled and compared with data from literature. It is found that when the maximum of the $4f^55d \rightarrow 4f^6$ emission wavelength is shorter than 730 nm, the probability to find an excited Sm^{2+} in the $4f^6[^5D_0]$ state becomes large enough that it lengthens the decay time of the $4f^55d \rightarrow 4f^6$ emission. This effect becomes more pronounced at shorter $4f^55d \rightarrow 4f^6$ emission wavelengths. Experimental evidence is also provided which shows that the model can be applied to the $4f^65d$ and $4f^7[^6P_{7/2}]$ levels of Eu^{2+}. The $4f^65d \rightarrow 4f^7$ decay time becomes longer when its emission wavelength is shorter than 400 nm. For Pr^{3+}, it is predicted that the $4f^15d \rightarrow 4f^2$ decay time becomes longer below 220 nm.

The model is used to explain large variations in the temperature dependence of the Sm^{2+} $4f^55d \rightarrow 4f^6$ emission decay time. When the $4f^55d$ level lies above the $4f^6[^5D_0]$ level, the $4f^6[^5D_0]$ level is primarily populated at low temperatures. Luminescence decay becomes faster upon increase of temperature as the $4f^55d$ level is thermally populated. The total change in decay time can be as large as 3 orders of magnitude. When the $4f^55d$ level lies below the $4f^6[^5D_0]$ level, the luminescence decay becomes slower upon increase of temperature. In both scenarios, the rate at which the decay time changes with temperature scales approximately with the inverse of the energy difference between the $4f^55d$ and $4f^6[^5D_0]$ levels, meaning faster changes are observed when the two levels lie close together. This information can be used for the development of luminescent thermometers.

For near-infrared scintillators, it has been determined that the decay time becomes too long when the $4f^55d \rightarrow 4f^6$ emission wavelengths are shorter than 730 nm. When the emission wavelength becomes longer than 800 nm, unrecoverable losses will occur in silicon based photodetectors. Therefore the optimal wavelength window for Sm^{2+}-doped near-infared scintillators is between 730 nm and 800 nm.

CRediT authorship contribution statement

Casper van Aarle: Conceptualization, Investigation, Visualization, Writing – original draft. **Karl W. Krämer:** Resources, Writing – review & editing. **Pieter Dorenbos:** Funding acquisition, Writing – review & editing.

Declaration of competing interest

The authors declare that they have no known competing financial interests or personal relationships that could have appeared to influence the work reported in this paper.

Data availability

Data will be made available on request.

Acknowledgements

This research was subsidized by the TTW/OTP grant no. 18040 of the Dutch Research Council. The authors would like to thank Daniel Biner, Bern, for the synthesis and crystal growth of the materials.

References

[1] D.L. Wood, W. Kaiser, Phys. Rev. 126 (1962) 2079.
[2] G. Baldini, M. Cartoceti, M. Guzzi, Solid State Commun. 8 (1970) 1697.
[3] M. Guzzi, G. Baldini, J. Lumin. 6 (1973) 270.
[4] R. Jaaniso, H. Bill, Europhys. Lett. 16 (1991) 569.
[5] Changjiang Wei, Keith Holliday, Alfred J. Meixner, Mauro Croci, Urs P. Wild, J. Lumin. 50 (1991) 89.
[6] W. Kaiser, C.G.B. Garrett, D.L. Wood, Phys. Rev. 123 (1961) 766.
[7] V.K. Koniukhov, V. Marchenko, A. Prokhorov, IEEE J. Quantum Electron. 2 (1966) 541.
[8] Yu.A. Anan'ev, A.A. Mak, B.M. Sedov, J. Exp. Theor. Phys. (U.S.S.R.) 52 (1967) 12.
[9] Hans Riesen, Wieslaw A. Kaczmarek, Inorg. Chem. 46 (2007) 7235.
[10] Go Okada, Noriaki Ikenaga, Yasuhiro Koguchi, Takayuki Yanagida, Safa Kasap, Hidehito Nanto, Mater. Res. Bull. 159 (2023) 112107.
[11] David de Vries, Sadiq van Overbeek, Evert P.J. Merkx, Erik van der Kolk, J. Lumin. 225 (2020) 117321.
[12] L.J.B. Erasmus, P.F. Smet, R.E. Kroon, D. Poelman, J.J. Terblans, J.J. Joos, D. Van der Heggen, H.C. Swart, ACS Photonics 10 (2023) 609.
[13] A. Lacam, C. Chateau, J. Appl. Phys. 66 (1989) 366.
[14] Paola Comodi, Pier Francesco Zanazzi, J. Appl. Crystallogr. 26 (1993) 843.
[15] Teng Zheng, Marcin Runowski, Przemysław Woźny, Stefan Lis, Victor Lavin, J. Mater. Chem. C 8 (2020) 4810.
[16] Laura Catherine Dixie, Andrew Edgar, Colin Murray Bartle, Nucl. Instrum. Methods A 753 (2014) 131.

[17] R.H.P. Awater, M.S. Alekhin, D.A. Biner, K.W. Krämer, P. Dorenbos, J. Lumin. 212 (2019) 1.
[18] Weronika Wolszczak, Karl W. Krämer, Pieter Dorenbos, Phys. Status Solidi R 13 (2019) 1900158.
[19] Daisuke Nakauchi, Yutaka Fujimoto, Takumi Kato, Noriaki Kawaguchi, Takayuki Yanagida, Crystals 12 (2022) 517.
[20] Claudio Yamamoto Morassuti, Simone Finoto, Junior Reis Silva, Sandro Marcio Lima, Luis Humberto da Cunha Andrade, Phys. Status Solidi B 257 (2020) 1900484.
[21] Aleksandar Ćirić, Stevan Stojadinović, Zoran Ristić, Ivana Zeković, Sanja Kuzman, Željka Antić, Miroslav D. Dramićanin, Adv. Mater. Technol. 6 (2021) 2001201.
[22] Chenwei Xu, Chenxia Li, Degang Deng, Jianxun Lu, Hua Yu, Le Wang, Xufeng Jing, Shiqing Xu, Chunxu Shao, Inorg. Chem. 61 (2022) 7989.
[23] P. Dorenbos, J. Phys. Condens. Matter 15 (2003) 575.
[24] Jianghao Xiong, Mingshu Zhao, Xiaotian Han, Zhongmin Cao, Xiantao Wei, Yonghu Chen, Changkui Duan, Min Yin, Sci. Rep. 7 (2017) 41311.
[25] Benedikt Bendel, Markus Suta, J. Mater. Chem. C 10 (2022) 13805.
[26] Zhongmin Cao, Xiantao Wei, Lu Zhao, Yonghu Chen, Min Yin, ACS Appl. Mater. Interfaces 8 (2016) 34546.
[27] Francis K. Fong, Howard V. Lauer, Charles R. Chilver, J. Chem. Phys. 63 (1975) 366.
[28] Laura C. Dixie, Andrew Edgar, Michael F. Reid, J. Lumin. 132 (2012) 2775.
[29] Pieter Dorenbos, Opt. Mater. X 1 (2019) 100021.
[30] Mikhail S. Alekhin, Roy H.P. Awater, Daniel A. Biner, Karl W. Krämer, Johan T.M. de Haas, Pieter Dorenbos, J. Lumin. 167 (2015) 347.
[31] T.C. Schäfer, J.R. Sorg, A.E. Sedykh, K. Müller-Buschbaum, Chem. Commun. 57 (2021) 11984.
[32] P.P. Feofilov, N.M. Tolstoi, Opt. Spectrosc. 13 (1962) 164.
[33] A.S.M. Mahbub'ul Alam, B. Di Bartolo, Phys. Lett. A 25 (1967) 157.
[34] L.L. Chase, Stephen A. Payne, Gary D. Wilke, J. Phys. C Solid State 20 (1987) 953.
[35] Mirosław Karbowiak, Piotr Solarz, Radosław Lisiecki, Witold Ryba-Romanowski, J. Lumin. 195 (2018) 159.
[36] J.L. Sommerdijk, J.M.P.J. Verstegen, A. Bril, J. Lumin. 8 (1974) 502.
[37] J. Sytsma, G. Blasse, J. Lumin. 51 (1992) 283.
[38] J.M.P.J. Verstegen, J.L. Sommerdijk, J. Lumin. 9 (1974) 297.
[39] J.L. Sommerdijk, A. Bril, J. Lumin. 11 (1976) 363.
[40] D.K. Sardar, W.A. Sibley, R. Alcala, J. Lumin. 27 (1982) 401.
[41] R. Alcala, D.K. Sardar, W.A. Sibley, J. Lumin. 27 (1982) 273.
[42] S. Mahlik, K. Wisniewski, M. Grinberg, Hyo Jin Seo, J. Non-Cryst. Solids 356 (2010) 1888.
[43] J.J. Schuyt, G.V.M. Williams, J. Lumin. 204 (2018) 472.
[44] R.A. Hewes, M.V. Hoffman, J. Lumin. 3 (1971) 261.
[45] J.P. Spoonhower, M.S. Burberry, J. Lumin. 43 (1989) 221.
[46] S.H.M. Poort, A. Meijerink, G. Blasse, J. Phys. Chem. Solids 58 (9) (1997) 1451.
[47] A. Meijerink, J. Lumin. 55 (1993) 125.
[48] D. Dutczak, T. Jüstel, C. Ronda, A. Meijerink, Phys. Chem. Chem. Phys. 17 (2015) 15236.
[49] Sadao Adachi, ECS J. Solid State Sci. Technol. 12 (2023) 016002.
[50] Fangtian You, Shihua Huang, Chunxia Meng, Dawei Wang, Jianhua Xu, Yan Huang, Guobin Zhang, J. Lumin. 122–123 (2007) 58.
[51] A.M. Srivastava, A.A. Setlur, H.A. Comanzo, M.E. Hannah, P.A. Schmidt, U. Happek, J. Lumin. 129 (2009) 126.
[52] A.M. Srivastava, A.A. Setlur, H.A. Comanzo, W.W. Beers, U. Happek, P. Schmidt, Opt. Mater. 23 (2011) 292.
[53] L.R. Elias, Wm.S. Heaps, W.M. Yen, Phys. Rev. B 8 (1973) 4989.
[54] P.A. Rodnyi, P. Dorenbos, G.B. Stryganyuk, A.S. Voloshinovskii, A.S. Potapov, C.W.E. van Eijk, J. Phys. Condens. Matter 15 (2003) 719.
[55] P. Vergeer, V. Babin, A. Meijerink, J. Lumin. 114 (2005) 267.
[56] E. van der Kolk, P. Dorenbos, C.W.E. van Eijk, A.P. Vink, C. Fouassier, F. Guillen, J. Lumin. 97 (2002) 212.
[57] R. Pappalardo, J. Lumin. 14 (1976) 159.
[58] A.M. Srivastava, D.A. Doughty, W.W. Beers, J. Electrochem. Soc. 142 (1996) 4113.
[59] S. Kück, I. Sokólska, M. Henke, M. Döring, T. Scheffler, J. Lumin. 102–103 (2003) 176.
[60] M. Nikl, H. Ogino, A. Yoshikawa, E. Mihokova, J. Pejchal, A. Beitlerova, A. Novoselov, T. Fukuda, Chem. Phys. Lett. 410 (2005) 218.
[61] M. Trevisani, K.V. Ivanovskikh, F. Piccinelli, A. Speghini, M. Bettinelli, ECS Trans. 41 (37) (2012) 11.
[62] Vladimir A. Pustovarov, Konstantin V. Ivanovskikh, Yulya E. Khatchenko, Qiufeng Shi, Marco Bettinelli, Radiat. Meas. 123 (2019) 39.
[63] A.M. Srivastava, J. Lumin. 169 (2016) 445.
[64] P. Dorenbos, J. Lumin. 104 (2003) 239.
[65] Aleksander Zych, Matthijs de Lange, Celso de Mello Donegá, Andries Meijerink, J. Appl. Phys. 112 (2012) 013536.
[66] Casper van Aarle, Karl W. Krämer, Pieter Dorenbos, J. Lumin. 238 (2021) 118257.
[67] Casper van Aarle, Karl W. Krämer, Pieter Dorenbos, J. Lumin. 251 (2022) 119209.
[68] Casper van Aarle, Karl W. Krämer, Pieter Dorenbos, J. Mater. Chem. C 11 (2023) 2336.
[69] W.J. Schipper, G. Blasse, J. Lumin. 59 (1994) 377.
[70] P. Dorenbos, J. Phys. Condens. Matter 15 (2003) 4797.
[71] P. Dorenbos, J. Lumin. 91 (2000) 155.
[72] G. Meyer, Advances in the Synthesis and Reactivity of Solids, vol. 2, JAI Press Inc., 1994, pp. 1–16.
[73] D. Sofich, R. Shendrik, A. Rusakov, A. Shalaev, A. Myasnikova, AIP Conf. Proc. 2392 (2021) 040004.
[74] Zhi-yi He, Yong-shen Wang, Sun Li, Xu-rong Xu, J. Lumin. 97 (2002) 102.
[75] Laura C. Dixie, Samarium doped alkaline Earth halides as red-emitting scintillators and phosphors, Thesis, Victoria University of Wellington, 2013, https://doi.org/10.26686/wgtn.17005837.v1.
[76] Mitsuo Yamaga, Shin-ichiro Tsuda, Jon-Paul R. Wells, Thomas P.J. Han, J. Ceram. Process. Res. 15 (2014) 167.
[77] T. Penhouet, H. Hagemann, J. Alloys Compd. 451 (2008) 74.
[78] Prodipta Pal, Tiphaine Penhouët, Vincenza D'Anna, Hans Hagemann, J. Lumin. 142 (2013) 66.
[79] Laura C. Dixie, Andrew Edgar, Murray C. Bartle, J. Lumin. 149 (2014) 91.
[80] Go Okada, Yutaka Fujimoto, Hironori Tanaka, Safa Kasap, Takayuki Yanagida, J. Rare Earths 34 (2016) 769.
[81] Yanlin Huang, Weifang Kai, Yonggang Cao, Kiwan Jang, Ho Sueb Lee, Ilgon Kim, Eunjin Cho, J. Appl. Phys. 103 (2008) 053501.
[82] W.J. Schipper, G. Blasse, J. Solid State Chem. 94 (1991) 418.
[83] J.L. Sommerdijk, P. Vries, A. Bril, Philips J. Res. 33 (1978) 117.
[84] Małgorzata Sójka, Marcin Runowski, Teng Zheng, Andrii Shyichuk, Dagmara Kulesza, Eugeniusz Zych, Stefan Lis, J. Mater. Chem. C 10 (2022) 1220.
[85] Takao Kobayasi, Stanley Mroczkowski, James F. Owen, Lothar H. Brixner, J. Lumin. 21 (1980) 247.
[86] Jin He, Rui Shi, Zhiqiang Wang, Minsi Li, Tsun-Kong Sham, Lianshe Fu, Adv. Opt. Mater. 10 (2022) 2101751.
[87] J.M.P.J. Verstegen, J.L. Sommerdijk, A. Bril, J. Lumin. 9 (1974) 420.
[88] Jarek Glodo, Edgar V. van Loef, Nerine J. Cherepy, Stephen A. Payne Kanai, S. Shah, IEEE Trans. Nucl. Sci. 57 (2010) 1228.
[89] Mikhail S. Alekhin, Daniel A. Biner, Karl W. Krämer, Pieter Dorenbos, J. Lumin. 145 (2014) 723.
[90] Daniel Rutstrom, Luis Stand, Merry Koschan, Charles L. Melcher, Mariya Zhuravleva, J. Lumin. 216 (2019) 116740.
[91] C. Barthou, R.B. Jabbarov, P. Benalloul, C. Chartier, N.N. Musayeva, B.G. Tagiev, O.B. Tagiev, J. Electrochem. Soc. 153 (2006) G253.
[92] V. Jarý, L. Havlák, J. Bárta, E. Mihóková, M. Nikl, Chem. Phys. Lett. 574 (2013) 61.
[93] U. Happek, M. Aycibin, A.M. Srivastava, H.A. Comanzo, S. Camardello, ECS Trans. 25 (2009) 39.
[94] C. Chartier, C. Barthou, P. Benalloul, J.M. Frigerio, J. Lumin. 111 (2005) 147.
[95] Paul Benalloul, Carlos Barthou, Claude Fouassier, Anatoly N. Georgobiani, Leonid S. Lepnev, Yusuf N. Emirov, Alex N. Gruzintsev, Bakhadur G. Tagiev, Oktay.B. Tagiev, Rasim.B. Jabbarov, J. Electrochem. Soc. 150 (2003) G62.
[96] Hong He, Renli Fu, Yongge Cao, Xiufeng Song, Zhengwei Pan, Xinran Zhao, Qingbo Xiao, Ran Li, Opt. Mater. 32 (2010) 632.
[97] Hyun Kyoung Yang, Hyeon Mi Noh, Byung Kee Moon, Jung Hyun Jeong, Soung Soo Yi, Ceram. Int. 40 (2014) 12503.
[98] Jianwei Qiao, Lixin Ning, Maxim S. Molokeev, Yu-Chun Chuang, Qinyuan Zhang, Kenneth R. Poeppelmeier, Zhiguo Xia, Angew. Chem. 131 (2019) 11645.
[99] A. Meijerink, J. Nuyten, G. Blasse, J. Lumin. 44 (1989) 19.
[100] Teng Zheng, Małgorzata Sójka, Przemysław Woźny, Inocencio R. Martín, Víctor Lavín, Eugeniusz Zych, Stefan Lis, Peng Du, Laihui Luo, Marcin Runowski, Adv. Opt. Mater. 10 (2022) 2201055.
[101] W. Wolszczak, K.W. Krämer, P. Dorenbos, J. Lumin. 222 (2020) 117101.
[102] Johan T.M. de Haas, Pieter Dorenbos, IEEE Trans. Nucl. Sci. 55 (2008) 1086.